Journal of the Korean Physical Society, Vol. 52, No. 2, February 2008, pp. 203∼208

Dynamic Phase Transition of the Globally-Coupled Kinetic Ising Model in the Low-Frequency Region

Beom Jun Kim
Department of Physics, BK21 Physics Research Division and Institute of Basic Science, Sungkyunkwan University, Suwon 440-746

Hyunsuk Hong*
Department of Physics and Research Institute of Physics and Chemistry, Chonbuk National University, Jeonju 561-756

(Received 19 November 2007, in final form 11 December 2007)

We revisit the globally-coupled kinetic Ising model in the presence of an oscillating external magnetic field with an amplitude h_0 and a driving angular frequency Ω. In the low-frequency region $\Omega \to 0$, the dynamic phase transition is shown to become discontinuous, and the phase boundary is found to be described by $h_0 \sim (1-T)^{3/2}$ with the temperature T and a critical temperature of unity in the limit $h_0 \to 0$. Our result is complementary to $h_0 \sim (1-T)^{1/2}$, previously known for the other limit $(1-T) \ll \Omega$. We extend the existing analytic calculation for the continuous transition to the second-order perturbation expansion and find that the dynamic phase transition occurs at lower temperature than the static one, which was not captured by the existing first-order calculation. The stochastic resonance behavior is also discussed in relation to the nature of the dynamic phase transition.

PACS numbers: 05.50.+q, 64.60.Cn, 05.70.Fh, 75.10.Hk
Keywords: Kinetic Ising model, Dynamic phase transition, Glauber dynamics

I. INTRODUCTION

The globally-coupled kinetic Ising model has been studied much due to its interesting dynamical behaviors, such as a dynamic phase transition, a stochastic resonance, the existence of hysteresis loop, and so on [1–6]. Not only is it an interesting system from a pure theoretical point of view, the kinetic Ising model in finite dimensions can also be used to describe experimental observations [7].

In the present work, we analyze the Glauber dynamics and obtain the phase boundaries in the plane of an external oscillating magnetic field and the temperature at various external driving frequencies. We show that as either the temperature is raised or the external oscillating field becomes larger, the system changes from ferromagnetic to paramagnetic, indicating that the oscillating field also enhances fluctuations similar to thermal fluctuations. After this confirmation of existing studies, we then focus on the low-frequency region for which the numerically obtained phase boundary via the direct integration of the equation of motion is shown to agree with the result from our adiabatic approximation. Via the second-order perturbation expansion, the relation between the static transition temperature T_s for the Ising model without time-varying external field ($h(t) = 0$) and the dynamic transition temperature T_d for the kinetic Ising model ($h(t) \neq 0$) is also explored. We finally investigate the occupancy ratio (OR), signaling the stochastic resonance behavior, which shows a very different behavior as the transition nature changes from continuous to discontinuous.

The present paper is organized as follows: Section II introduces the system of the globally-coupled kinetic Ising model with an oscillatory magnetic field. In Section III, the dynamic order parameter is defined and is used to obtain the phase boundaries at different external frequencies. The method of the adiabatic approximation is described in detail, and its result is compared with numerical ones. Section IV is devoted to the second-order perturbation expansion applied for the critical region, which is followed by Section V, in which the occupancy ratio is discussed. Finally, the main results are summarized in Section VI.

II. GLOBALLY-COUPLED KINETIC ISING MODEL

We begin with the globally-coupled kinetic Ising model defined by the Hamiltonian

*Corresponding Author: hhong@chonbuk.ac.kr

$$H = -\frac{J}{N}\sum_{i<j}\sigma_i\sigma_j - h(t)\sum_{i=1}^{N}\sigma_i, \quad (1)$$

where N is the total number of spins, $\sigma_i = \pm 1$ is the spin variable at the ith site, $J(>0)$ is the strength of the ferromagnetic interaction, and $h(t) = h_0 \sin \Omega t$ is the oscillatory magnetic field with magnitude h_0 and driving frequency Ω. The neighboring spins energetically favor pointing in the same direction due the ferromagnetic interaction $J > 0$; however, different from the static field, the oscillating field $h(t)$ drives the spins to change their directions in time. The globally-coupled kinetic Ising model subject to the Glauber dynamics is conveniently described by the equation of motion (see Ref. 2 for more details).

$$\frac{dm(t)}{dt} = -m(t) + \tanh\left(\frac{m(t)+h(t)}{T}\right), \quad (2)$$

where T is the temperature in units of J/k_B, the oscillating field $h(t)$ is in units of J, and the magnetization $m(t)$ is the ensemble average of a spin at time t. It should be noted that the equation of motion, Eq. (2), is exact within the continuous time approximation, in which the discrete time in the Glauber dynamics is approximated to be continuous.

When there is no external field in the system ($h(t) = 0$), the interaction between the spins competes with the thermal noise with strength T. If the interaction is strong enough to overcome the thermal noise, macroscopic magnetic ordering appears, and the system reveals a phase transition from a randomly disordered phase to an ordered one as the temperature is decreased. We note that the low-temperature phase has a spontaneously broken symmetry and that the high-temperature one has a fully-disordered random phase without any ordering. In the mean-field scheme, this transition is known to occur exactly at $T = T_s = 1$. Henceforth, we use the symbol T_s to denote the transition temperature for the static case with $h_0 = 0$. In the presence of an external field ($h(t) \neq 0$), on the other hand, the system is known to exhibit a dynamic phase transition, and various aspects, such as the existence of a tricritical point, have already been studied [1–4]. We below focus on the dynamic phase transition in the low-frequency region.

III. DYNAMIC PHASE TRANSITION: ADIABATIC LIMIT

In this section, we investigate the dynamic phase transition by using Q_n defined by

$$Q_n \equiv \frac{\Omega}{2\pi}\int_{2\pi n/\Omega}^{2\pi(n+1)/\Omega} dt m(t). \quad (3)$$

If the system achieves its stationary state, Q_n does not depend on n anymore, and we define the dynamic order parameter Q as

$$Q \equiv \lim_{n\to\infty} Q_n. \quad (4)$$

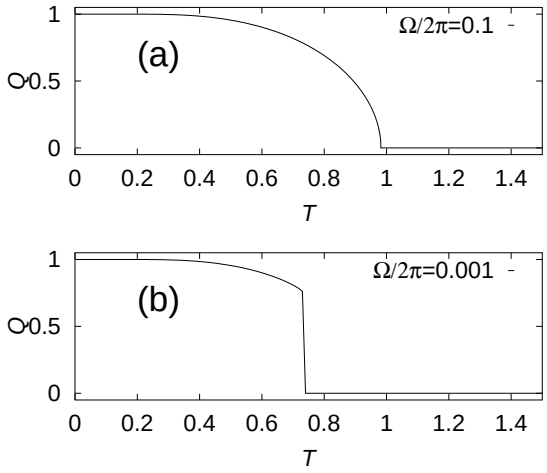

Fig. 1. Dynamic order parameter Q vs. temperature T at $h_0 = 0.1$ for (a) $\Omega/2\pi = 0.1$ and (b) $\Omega/2\pi = 0.001$. The dynamic phase transition changes its nature from continuous (at $\Omega/2\pi = 0.1$) to discontinuous (at $\Omega/2\pi = 0.001$) as Ω is decreased.

In our numerical simulations, we integrate Eq. (2) over time by using the second-order Runge-Kutta method with the time step $dt = 0.01$ for given values of the amplitude h_0 and the angular frequency Ω of the external oscillating field, $h(t) = h_0 \sin \Omega t$. The numerical integration is performed first at a sufficiently high temperature, and at each given temperature, the magnetization $m(t)$ for the first 200 periods ($2\pi/\Omega$) is discarded to ensure the equilibration, and measurements are made for the next 200 periods. We anneal the system by decreasing T slowly, trying to make the system settle down only at one dynamic fixed point.

Figure 1 shows the behavior of Q as a function of temperature T at $h_0 = 0.1$ for (a) $\Omega/2\pi = 0.1$ and (b) $\Omega/2\pi = 0.001$. The dynamic order parameter Q clearly detects the existence of the phase transition: ferromagnetic at low temperatures and paramagnetic at high temperatures. The phase transition changes its nature from a continuous transition to a discontinuous one as Ω is decreased. We repeat similar calculations at various values of h_0 and Ω, and detect the dynamic phase transition point when Q first becomes larger than 0.001 as T is lowered from a sufficiently high temperature. (The choice other than 0.001, if not too different, does not make a significant difference in the estimate of the transition temperature). In Figure 2, we show the phase boundaries in the (T, h_0) plane at various values of Ω. As the temperature is lowered, the system is seen to change from paramagnetic ($Q = 0$) to ferromagnetic ($Q \neq 0$), as expected. If the temperature is fixed, but the amplitude h_0 of the oscillating magnetic field is increased,

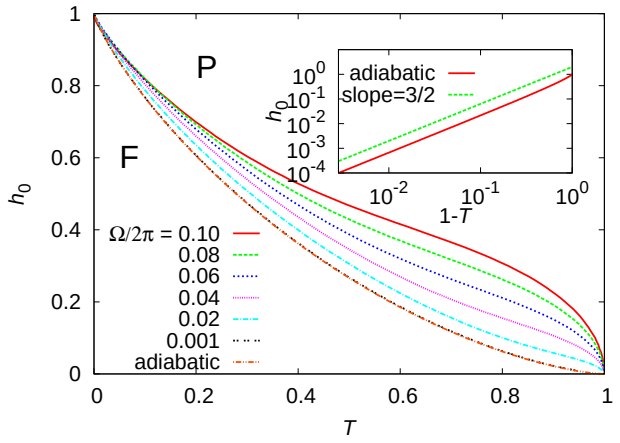

Fig. 2. (Color online) Phase boundaries in the (h_0, T) plane at various values of the external driving frequency Ω. As Ω decreases, the numerically obtained phase boundary approaches the one computed via the adiabatic approximation (see the text). Inset: Phase boundary calculated from the adiabatic approximation ($\Omega \ll 1$) is plotted as h_0 vs. $1-T$ on a log-log scale. Over a broad range of temperatures, $h_0 \sim (1-T)^{3/2}$ is found to fit well.

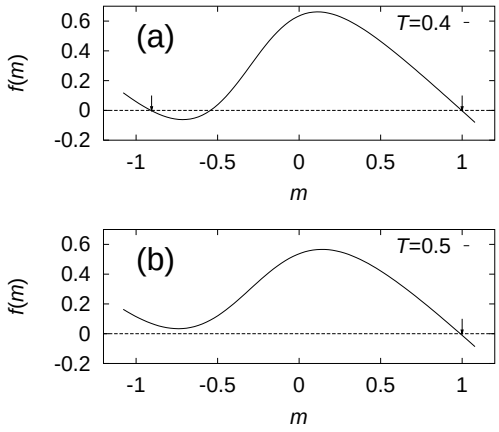

Fig. 3. Stability analysis of Eq. (2) within the adiabatic approximation [$f(m)$ is the right-hand side of Eq. (2) with $h(t) = 0.3$]. (a) At low temperatures, there exist two stable fixed points, one of which has a plus sign and the other a minus sign (denoted by small arrows). (b) As the temperature is increased, one of the two stable fixed points disappears at the critical temperature. It is clear that this mechanism gives rise to a discontinuous phase transition instead of a continuous one.

the system also changes from ferromagnetic to paramagnetic, implying that a bigger oscillating magnetic field provides stronger fluctuation. In the present paper, we study in detail the case of $\Omega \ll 1$, for which the adiabatic approximation becomes valid. In other words, the external driving is assumed to vary so slowly that we assume that one can decouple the time scale related with $m(t)$ from the one related with $h(t)$. Within this adiabatic approximation, $m(t)$ approaches the dynamic fixed point of Eq. (2) very rapidly and stays there for a long time. Consequently, the dynamic phase transition point is simply determined from a fixed-point analysis of the right-hand side of Eq. (2), which we call $f(m)$. At sufficiently low temperatures, the symmetry is spontaneously broken, and there exist two stable fixed points for Eq. (2), one of which has a negative and the other a positive value of m, as displayed in Figure 3(a). Once the system is at one of the fixed point, it does not move to other fixed point although $h(t)$ changes; it is to be noted that the thermal fluctuation has already been integrated to yield Eq. (2) and that no mechanism to make the transition between fixed points, overcoming the free-energy barrier, is possible. Accordingly, as $h(t)$ changes (although very slowly), $m(t)$ keeps one of the signs, positive or negative, depending on the initial condition, resulting in $Q \neq 0$. In contrast, as T becomes higher, the above behavior changes, as displayed in Figure 3(b): At a given value of $h(t)$, the system is shown to have only one stable fixed point. As $h(t)$ is changed, the unique fixed point also changes slowly, covering a broad range of m including both sides of zero. Accordingly, at sufficiently high temperatures, the time-averaged value of $m(t)$ becomes zero, giving $Q = 0$. From this simple stability analysis, it is straightforward to estimate the dynamic phase transition temperature T_d: We only need to pick the parameter at which the number of fixed points changes from two to one. The curve marked as 'adiabatic' in Figure 2 corresponds to the phase boundary via the stability analysis within this adiabatic approximation. The numerically obtained phase boundary at $\Omega/2\pi = 0.001$ is clearly shown to exhibit perfect agreement with the one found from the adiabatic approximation. We also emphasize that the above mechanism of the phase transition in the adiabatic limit naturally explains the phase transition being discontinuous: The change from two fixed points to a single one, corresponding to that from Figure 3(a) to Figure 3(b), does not occur in a continuous way.

As the frequency goes to zero, we find that in a broad range of temperatures,

$$h_0 \sim (1-T)^{3/2} \tag{5}$$

well describes the phase boundary, as shown in the inset of Figure 2. The exponent $a = 3/2$ of $h_0 \sim (1-T)^a$ in the limit of $\Omega \to 0$ can be understood from a simple static argument: The mean-field values of the static critical exponents $\beta = 1/2$ in $m \sim (1-T)^\beta$ and $\delta = 3$ in $h \sim m^\delta$ lead to $h \sim (1-T)^{\beta\delta} \sim (1-T)^{3/2}$. We note that, in contrast, in Ref. 3, the phase boundary satisfying

$$h_0 \approx \left(\frac{2\Omega^2}{1+\Omega^2}\right)^{1/2} (1-T)^{1/2} \tag{6}$$

is obtained for $(1-T) \ll \Omega$. In the small-frequency region ($\Omega \ll 1$) where the behavior in Eq. (5) is obeyed, the condition $(1-T) \ll \Omega$, which Eq. (6) is based on, is not

valid anymore. The two results given by Eq. (5) and (6) are complementary to each other, corresponding to different regions of the driving frequency Ω: the adiabatic region ($\Omega \ll 1$) and the critical region [$(1-T) \ll \Omega$]. Those two different exponents in Eq. (5) and (6), one larger and the other smaller than unity, are also expected from the different slopes of the phase boundary shown in Figure 2: As Ω goes to zero, dh_0/dT goes to zero near $T = 1$ while it tends to diverge as Ω becomes large near $T = 1$.

IV. SECOND-ORDER PERTURBATION EXPANSION

We next focus on the critical region and use the second-order perturbation expansion to study the dynamic phase transition. We start from Eq. (2) with the inverse temperature $\beta = 1/T$,

$$\frac{dm}{dt} = -m + \tan h(\beta m + \beta h), \tag{7}$$

consider first the first-order perturbation expansion up to the linear order in βh and write

$$m_1 = m_0 + \epsilon, \tag{8}$$

where m_0 is the zero-th order solution, *i.e.*, $m_0 = \tanh \beta m_0$ and ϵ satisfies

$$\frac{d\epsilon}{dt} = \Big(\beta F(\beta m_0) - 1\Big)\epsilon + \beta F(\beta m_0) h_0 \sin \Omega t, \tag{9}$$

with

$$F(\beta m_0) = \frac{e^{\beta m_0}}{\cosh \beta m_0}\Big(1 - \tanh \beta m_0\Big). \tag{10}$$

We then write the steady-state solution of Eq. (9) in the form

$$\epsilon = \epsilon_0 \sin(\Omega t - \theta), \tag{11}$$

where

$$\theta = \tan^{-1}\left(\frac{\Omega}{1-\beta F}\right),$$
$$\epsilon_0 = \frac{\beta F h_0}{\Omega \sin\theta + (1-\beta F)\cos\theta} \tag{12}$$

are obtained by using the linear independence property of the $\sin \Omega t$ and the $\cos \Omega t$ terms when the trial solution Eq. (11) satisfies Eq. (9).

The dynamic order parameter Q then reads

$$Q = \frac{\Omega}{2\pi}\int_{2\pi n/\Omega}^{2\pi(n+1)/\Omega} dt\big[m_0 + \epsilon_0 \sin(\Omega t - \theta)\big] = m_0. \tag{13}$$

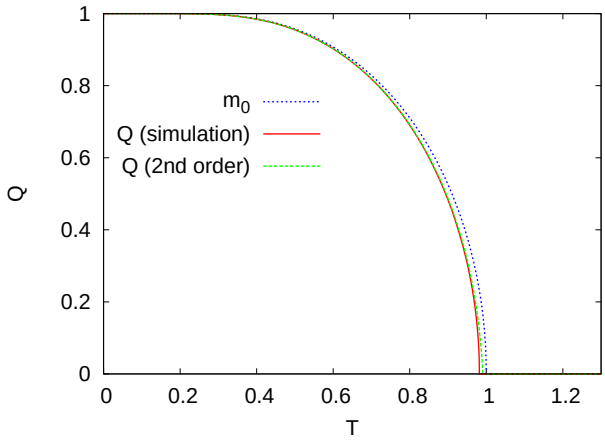

Fig. 4. (Color online) The dynamic order parameter Q versus the temperature T at $\Omega/2\pi = 0.1$ and $h_0 = 0.1$. The numerically computed value is shown to be significantly different from the static value m_0. On the other hand, the second-order perturbation calculation gives Q values very close to the actual ones.

We note the result shown in Eq. (13) implies that the first-order perturbation expansion in βh yields $T_d = T_s$, which is not consistent with the numerical observation shown in the previous studies [1,5].

To remedy such an inconsistency, let us now keep the second-order terms of $(\beta h)^2$. We now write the magnetization m as $m_2 = m_0 + y$ with $y = \epsilon + z$, where ϵ is the solution in the first-order expansion and z is the solution in the second-order expansion. Considering the expansion up to the second-order terms, we find

$$\frac{d}{dt}(\epsilon + z) = -(\epsilon + z) + \beta(\epsilon + z + h)F(\beta m_0) + \beta^2(\epsilon + z + h)^2 G(\beta m_0), \tag{14}$$

where

$$G(\beta m_0) = \frac{e^{\beta m_0}(1 - \tanh \beta m_0)}{\cosh \beta m_0} \times \left(1 - \frac{e^{\beta m_0}}{\cosh \beta m_0}\right), \tag{15}$$

which yields

$$\frac{dz}{dt} = \big[\beta F(\beta m_0) - 1\big]z + \beta^2 G(\beta m_0)\big[\epsilon_0 \sin(\Omega t - \theta) + h_0 \sin \Omega t\big]^2. \tag{16}$$

The solution of Eq. (16) is then given by

$$z(t) = e^{(\beta F - 1)(t - t_0)} \times \int_{t_0}^{t} dt' e^{(1-\beta F)t'} \beta^2 \big[\epsilon_0 \sin(\Omega t' - \theta) + h_0 \sin \Omega t'\big]^2,$$

which finally yields

$$Q = m_0 + \frac{\beta^2 G}{2(1-\beta F)}\Big|(\epsilon_0 \cos\theta + h_0)^2 + \epsilon_0^2 \sin^2\theta\Big|. \tag{17}$$

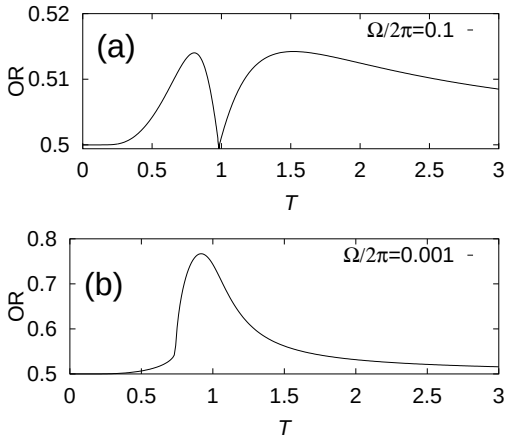

Fig. 5. Occupancy ratio OR vs. T at $h_0 = 0.1$ for (a) $\Omega/2\pi = 0.1$ and (b) $\Omega/2\pi = 0.001$. As we decrease Ω, OR exhibits a dramatic change: two peaks for large Ω where the phase transition is continuous, and only one peak for small Ω where it is discontinuous.

The dynamic phase transition temperature T_d can be found from the condition $Q = 0$. We note that G in Eq. (17) with Eq. (15) is always negative, which implies Q is always smaller than m_0. Accordingly, we expect the dynamic phase transition temperature T_d to be smaller than the static one T_s, which is consistent with the numerical observations [1,5]. In Figure 4, we compare the results from the first-order perturbation, which is nothing but the static value m_0, from the second-order calculation presented above, and from the actual numerical integration of the equation of motion. The second-order perturbation presented above is clearly seen to give values in good agreements with the actual ones.

V. OCCUPANCY RATIO

In this section, we investigate the behavior of another interesting quantity, the occupancy ratio OR defined by

$$\mathrm{OR} \equiv \left\langle \frac{\text{number of spins in the direction of } h(t)}{\text{total number of spines}} \right\rangle. \tag{18}$$

The OR measures how many spins follow the same direction as the external field $h(t)$. Figure 5(a) shows the behavior of the OR as a function of the temperature T for $h_0 = 0.1$ and $\Omega/2\pi = 0.1$, where two peaks clearly appear, one below and the other above T_d. The positions of these two peaks are $T \approx 0.8$ and $T \approx 1.5$ with $T_d \approx 0.98$.

The temperatures at which the OR exhibits maxima are well understood from the matching condition of the intrinsic and the extrinsic time scales when the dynamic phase transition is continuous [5]. In more detail, the magnetization of the system changes its sign in accord with the external magnetic field when the relaxation time τ of the system matches the external driving frequency, *i.e.*, $\tau \approx 1/\Omega$, as was shown in Ref. 5. Since the relaxation time diverges as T approaches the critical temperature both from below and above, the matching condition is satisfied at two different temperatures, one below and the other above T_d [5], which clearly explains the existence of double OR peaks in Figure 5(a). In contrast, it is seen in Figure 5(b) that in the low-frequency region where the phase transition becomes discontinuous, the OR exhibits only one single peak instead of double peaks. Furthermore, the OR maximum occurs in the paramagnetic phase ($T > T_d \approx 0.75$), which implies that the OR peak in the ferromagnetic phase [the left peak in Figure 5(a)] disappears as $\Omega \to 0$. In this low-frequency region, the magnetization $m(t)$ changes quasi-statically and, thus, is fully synchronized with the change of the external magnetic field in the paramagnetic phase. In the low-temperature phase, the spontaneously broken symmetry prohibits $m(t)$ from changing its sign in accord with $h(t)$, which explains the absence of the ferromagnetic OR peak in this case. Accordingly, we conclude that the number of peaks in the OR is closely related with the nature of the phase transition.

VI. SUMMARY

In this paper, we have investigated the globally-coupled kinetic Ising model with an oscillatory magnetic field, with particular attention paid to the dynamic phase transition and the low-frequency effects on it. The phase diagram splitting the ferromagnetic phase and the paramagnetic one has been constructed for various external driving frequencies, which agrees with the known result. We then focus on the phase boundary in the low-frequency limit $\Omega \to 0$, which exhibits $h_0 \sim (1-T)^{3/2}$ different from the other limiting case of $(1-T) \gg \Omega$ studied in Ref. 3. A simple adiabatic approximation has been proposed, which, combined with the stability analysis, gives good consistency with the phase boundary numerically obtained. Also, via the second-order perturbation expansion, we explain that the dynamic transition occurs at a lower temperature than the static one ($T_d < T_s$). The occupancy ratio is also considered, and a correlation between the transition nature and the number of OR peaks is suggested.

ACKNOWLEDGMENTS

This work was supported by a Korea Research Foundation grant funded by the Korean Government (MOEHRD), grant Nos KRF-2006-312-C00548 (B. J. K) and KRF-2006-331-C00123 (H. H).

REFERENCES

[1] B. K. Chakrabarti and M. Acharyya, Rev. Mod. Phys. **71**, 847 (1999); W. S. Lo and R. A. Pelcovits, Phys. Rev. A **42**, 7471 (1990); M. Acharyya and B. K. Chakrabarti, Phys. Rev. B **52**, 6550 (1995); S. W. Sides, P. A. Rikvold and M. A. Novotny, Phys. Rev. Lett. **81**, 834 (1998); *ibid.,* Phys. Rev. E **59** 2710 (1999); M. Acharyya, Phys. Rev. E **56** 1234 (1997); 2407 (1997).
[2] K. Leung and Z. Néda, Phys. Lett. A **246**, 505 (1998).
[3] T. Tomé and M. J. de Oliveira, Phys. Rev. A **41**, 4251 (1990).
[4] M. Acharyya, Phys. Rev. E **59**, 218 (1999).
[5] B. J. Kim, P. Minnhagen, H. J. Kim, M. Y. Choi and G. S. Jeon, Europhys Lett. **56**, 333 (2001).
[6] S. K. Oh, C. N. Yoon, J. S. Chung and H. J. Kang, J. Korean Phys. Soc. **37**, 503 (2000); S. K. Oh and H. J. Kang, *ibid.*, **47**, 6 (2005); S. K. Oh, *ibid.*, **48**, 18 (2006); H. Hong, H. Park and L.-H. Tang, *ibid.*, **49**, L1885 (2006); J. Um, S.-I. Lee and B. J. Kim, *ibid.*, **50**, 285 (2007).
[7] Z. Zhu, Y. Sun, Q. Zhang and J.-M. Liu, Phys. Rev. B **76**, 014439 (2007).